

PCCP

Accepted Manuscript



This is an *Accepted Manuscript*, which has been through the Royal Society of Chemistry peer review process and has been accepted for publication.

Accepted Manuscripts are published online shortly after acceptance, before technical editing, formatting and proof reading. Using this free service, authors can make their results available to the community, in citable form, before we publish the edited article. We will replace this *Accepted Manuscript* with the edited and formatted *Advance Article* as soon as it is available.

You can find more information about *Accepted Manuscripts* in the [Information for Authors](#).

Please note that technical editing may introduce minor changes to the text and/or graphics, which may alter content. The journal's standard [Terms & Conditions](#) and the [Ethical guidelines](#) still apply. In no event shall the Royal Society of Chemistry be held responsible for any errors or omissions in this *Accepted Manuscript* or any consequences arising from the use of any information it contains.

**Facile hydrothermal synthesis of NiMoO₄@CoMoO₄ hierarchical
nanospheres for supercapacitor applications**

Zhen Zhang, Yundan Liu, Zongyu Huang*, Long Ren, Xiang Qi*, Xiaolin Wei,

Jianxin Zhong

*Hunan Key Laboratory of Micro-Nano Energy Materials and Devices, Xiangtan
University, Hunan 411105, P.R. China, and Laboratory for Quantum Engineering and
Micro-Nano Energy Technology and School of Physics and Optoelectronics, Xiangtan
University, Hunan 411105, P. R. China*

* Corresponding author: School of Physics and Optoelectronics, Xiangtan University,

Hunan 411105, P. R. China

E-mail address: zyhuang@xtu.edu.cn, xqi@xtu.edu.cn

Abstract

Novel binder-free electrode material of NiMoO₄@CoMoO₄ hierarchical nanospheres anchored on nickel foam with excellent electrochemical performance has been synthesized via a facile hydrothermal strategy. Microstructures and morphologies of samples are characterized by X-ray diffraction (XRD), Raman, scanning electron microscope (SEM), transmission electron microscopy (TEM), energy dispersive spectroscope (EDS) and X-ray photoelectron spectroscopy (XPS). Besides, the effect of Ni/Co molar ratios of raw materials on electrochemical behaviors is also investigated by cyclic voltammetry, galvanostatic charge-discharge measurements, cycling tests and electrochemical impedance spectroscopy methods. Remarkably, the resulting NiMoO₄@CoMoO₄ hierarchical nanospheres with Ni/Co molar ratio of 4:1 exhibit greatly enhanced capacitive properties relative to other components and display a high specific capacitance of 1601.6 Fg⁻¹ at the current density of 2 Ag⁻¹, as well as better cycling stability and rate capability. Moreover, a symmetric supercapacitor is constructed using NiMoO₄@CoMoO₄ nanospheres as the positive and negative electrodes with one piece of cellulose paper as the separator, which shows good electrochemical performance. Such enhanced capacitive properties are mostly attributed to the synergistic effect of nickel and cobalt molybdates, directly deposition on conductive substrate and their novel hierarchical structure, which can provide pathways for fast diffusion and transportation of ions and electrons and a large number of active sites. The results imply that the NiMoO₄@CoMoO₄ hierarchical nanospheres could be a promising candidate for electrochemical energy storage.

Keywords: NiMoO₄@CoMoO₄, energy storage, supercapacitors

1. Introduction

Recently, in order to meet the increasing demand of rapid development of portable electronic devices and electrical vehicles, a significant amount of effort has been devoted to various emerging energy storage technologies. Electrochemical capacitors, also known as supercapacitors, are considered to be one of the most promising candidates for alternative energy storage, due to its many intriguing advantages, such as high power density, fast charge-discharge process, environmental friendliness and long cycling life.¹⁻⁴ According to the energy storage mechanism, supercapacitors are generally categorized into two main types: electrical double-layer capacitors (EDLCs), that store energy using ion adsorption on the surface of active materials and pseudocapacitors where capacitance comes from reversible Faradaic reactions taking place at the electrode/electrolyte interface.^{5,6} In contrast to the electrical double-layer capacitors, pseudocapacitors can provide much higher specific capacitance due to their fast and reversible redox reaction.^{7, 8} Generally, transition metal oxides, hydroxides and conducting polymers have relative higher capacitance and fast redox kinetics, which are considered as promising candidates for pseudocapacitors.⁹ For example, RuO₂ has been the most promising pseudocapacitive materials because of its good electrical conductivity and excellent power densities.¹⁰ However, the expensive nature and toxicity of ruthenium has hindered its widespread commercial applications. Therefore, it is still a great challenge to explore novel alternative and inexpensive electrode materials with appropriate electrochemical properties.

As the potential electrode materials for supercapacitors, binary transition metal oxides have attracted growing interest because of their abundant sources, environmental friendliness, much higher electrical conductivity and more excellent electrochemical activity resulting from the simultaneous effects of individual constituents.¹¹ More interestingly, among various BTMOs materials, metal molybdates, possessing multiple oxidation states and structures that enable multiple redox reaction, have demonstrated vastly improved electrochemical properties over single component oxides, which seem to be the most promising materials for

supercapacitors.^{12, 13} Mai et al. synthesized heterostructured $\text{MnMoO}_4\text{-CoMoO}_4$ nanowires by a simple refluxing method under mild conditions, which exhibit a specific capacitance of 181.7 Fg^{-1} at a current density of 1 Ag^{-1} .¹⁴ Worth the whistle, the main function of the Mo element is to improve the conductivity of metal molybdates and then to enhance electrochemical capacitance, but it does not participate in any redox reaction, thus showing no contribute to the specific capacitance.¹⁵ Nowadays, among metal molybdates, NiMoO_4 and CoMoO_4 are attracting growing interest.^{16, 17} Baskar et al. successfully prepared $\alpha\text{-NiMoO}_4$ nanoparticles via a solution combustion synthesis technique, which delivered a high specific capacitance of 1517 Fg^{-1} at a current density of 1.2 Ag^{-1} .¹⁸ Unfortunately, despite the high specific capacitance ascribed to the high electrochemical activity of nickel ion, the rate capability of NiMoO_4 is still undesirable for its wide practical applications. One-dimensional $\text{CoMoO}_4\cdot\text{H}_2\text{O/rGO}$ hybrid composites revealing a good rate capability were fabricated by Xu group via a simple and environmental hydrothermal synthesis method, which only achieved a inferior specific capacitance of 701.9 Fg^{-1} at a current density of 2 Ag^{-1} .¹⁹ Previous reports motivated us to fabricate and design a $\text{NiMoO}_4@\text{CoMoO}_4$ hybrid composite with novel nanostructure facilitating fast electrolyte ion transport, which might combine the advantages of both high specific capacitance originating from NiMoO_4 and excellent rate capability provided by CoMoO_4 .

More importantly, the traditional binder-contained electrodes are usually manufactured by slurry-coating technique, where the involved binder will greatly reduce the electrical conductivity of active materials and the introduction of conductive agent may lead to dead surface and an extra contact resistance between the current and electrode materials, thus hindering the fast electron transport and decreasing the utilization of active materials.²⁰ Facing these realities, an emerging attractive attempt is to directly grown pseudocapacitive materials nanostructure on conducting substrates used as binder-free electrodes. Typically, Ni foam (NF) is often selected as conductive substrate to sever as backbone, due to its three-dimensional open-pore and cross-linked grid structure, which facilitates easy access of electrolyte

ion into electrode.^{15, 21} Therefore, it is an effective strategy to directly grow binary transition metal oxides on NF substrate, which will avoid the use of polymer binder, efficiently reduce Ohmic polarization, provide faster kinetics and enhance the rate capability.

In this work, the NiMoO₄@CoMoO₄ hierarchical nanospheres are successfully grown on nickel foam via a simple and environmentally friendly hydrothermal synthesis approach. Combining the advantages of both NiMoO₄ and CoMoO₄, the as-prepared hybrid composite with Ni/Co molar ratio of 4:1 exhibits a high specific capacitance of 1601.6 Fg⁻¹ at the current density of 2 Ag⁻¹, as well as more excellent rate capability than that of individual metal molybdates. Meanwhile, a symmetric supercapacitor is assembled by using NiMoO₄@CoMoO₄ hierarchical nanospheres as both positive and negative electrode, which exhibits a good electrochemical behavior. Due to the remarkable electrochemical properties, simplicity facile synthetic approach and binder free electrode design, the resulting NiMoO₄@CoMoO₄ hierarchical nanospheres are generally considered as a promising electrode material for supercapacitors.

2. Experimental Section

2.1 Materials preparation

All the chemicals are used as received without further purification. NiMoO₄@CoMoO₄ hierarchical nanospheres have been synthesized by a simple hydrothermal process without any structure directing agents. Typically, a piece of nickel foam severed as conductive substrate (1 cm × 3 cm in a rectangular shape) is cleaned by concentrated HCl solution, acetone, ethanol and deionized water with assistance of ultrasonication for several minutes, and then is placed against the wall of a Teflon-lined stainless steel autoclave that contains a homogeneous solution of Ni(NO₃)₂·6H₂O, Co(NO₃)₂·6H₂O and Na₂MoO₄·2H₂O. To prepare solutions (total molar concentration of 5mmol/L⁻¹) with n(Ni)/n(Co) ratios of 10:0, 8:2, 5:5, 2:8, 0:10, controlled amount of Ni- and Co- containing reagents are dissolved in 25mL

deionized water under constant magnetic stirring, then $\text{Na}_2\text{MoO}_4 \cdot 2\text{H}_2\text{O}$ (5 mmol/L⁻¹) is added into the solution. Afterwards, the resulting solutions are transferred into the above Teflon-lined stainless steel autoclaves, sealed and maintained at 150 °C for 8 h, then allowed to cool room temperature naturally. The as-prepared precursor is taken out and washed several times with distilled water and ethanol before being fully dried at 60 °C overnight under vacuum and then annealed at 400 °C for 2 h. Finally, the mass loading of active materials with n(Ni)/n(Co) ratio of 8:2 is about 0.9 mg/cm². We fabricate the symmetric supercapacitors based on the $\text{NiMoO}_4 @ \text{CoMoO}_4$ with Ni/Co ratio of 4:1 on nickel foam. Both positive and negative electrodes are $\text{NiMoO}_4 @ \text{CoMoO}_4$ with the same mass, which are separated by one piece of cellulose paper.

2.2 Structural characterizations

The crystal structures of the as-prepared samples were determined by X-ray diffraction (XRD) using Cu K α radiation. Raman spectra were collected by using the Renishaw InVia Raman microscope, excited at room temperature with excitation laser wavelength of 532 nm. The morphologies and microstructures of the samples were characterized using transmission electron microscopy (TEM), and scanning electron microscopy (SEM, JEOL, JSM 6360) with an energy dispersive spectroscope (EDS). The surface chemical compositions are identified by X-ray photoelectron spectroscopy (XPS). N₂ adsorption-desorption is determined by Brunauer-Emmett-Teller (BET) measurements (TriStar 3020).

2.3 Electrochemical tests

The electrochemical properties of the as-obtained electrode material are investigated in a three-electrode configuration where the nickel foam covered with $\text{NiMoO}_4 @ \text{CoMoO}_4$ hierarchical nanospheres is directly used as working electrode, platinum foil and Ag/AgCl served as counter and reference electrodes, respectively. All the electrochemical measurements including cyclic voltammogram, galvanostatic charge/discharge test are carried out in 1 M KOH aqueous solution with a CHI660D (ChenHua, China) electrochemistry workstation. Electrochemical impedance

spectroscopy (EIS) measurement is also carried out in the frequency range of 100 kHz-0.01 Hz with perturbation amplitude of 5 mV.

3. Results and discussion

3.1 Structural and morphology characterization

In this work, NiMoO₄@CoMoO₄ hierarchical nanospheres are prepared by a simple hydrothermal process coupled with a calcinations treatment. Firstly, the NiMoO₄@CoMoO₄ precursor is anchored on the surface of nickel foam substrate by hydrothermal synthesis technique, which is dehydrated by the following annealing treatment to become NiMoO₄@CoMoO₄ hierarchical nanospheres. First of all, powder X-ray diffraction (XRD) measurements are carried out to gain insight into the internal structure of NiMoO₄@CoMoO₄ hierarchical nanospheres on NF substrate. In order to reduce the strong impact of the Ni foam substrates on the XRD peaks signals, the samples powder are scratched from nickel foam for XRD analysis, as shown in Figure 1(a). The patterns of single NiMoO₄ and pure CoMoO₄ are in good agreement with the standard patterns for NiMoO₄ (JCPDF card No. 86-0361) and CoMoO₄ (JCPDF card No. 21-0868), respectively. In addition, the diffraction peaks of both NiMoO₄ and CoMoO₄ phases are all observed in the patterns of NiMoO₄@CoMoO₄ hybrid nanospheres, indicating the coexist the NiMoO₄ and CoMoO₄. As for the hybrid composites, with the increase of Co concentration in raw material, peaks at around 14.3°, 28.2°, 32.7° and 43.7° attributed to the reflections of (110), (201), (022) and (330) planes for NiMoO₄ become weaken, and several peaks located at 13.2°, 23.2°, 26.3°, 31.8°, 33.5° and 36.5° (marked by black arrows) are gradually enhanced, which correspond to (001), (021), (002), (-131), (-222), and (400) planes for CoMoO₄. The poor crystallization results in more pathways for electrolyte penetration and ions transport than a material with good crystallinity, which are favorable for the nanocomposite to present an excellent capacitive behavior.¹² In order further explore the NiMoO₄@CoMoO₄ nanostructures, Raman tests are performed in this work. As shown in Figure 1(b), the Raman spectrum of pure NiMoO₄ exhibits an

intense peak at 961 cm^{-1} , along with some medium intensity peaks appearing at 912 cm^{-1} , 834 cm^{-1} , 709 cm^{-1} and 385 cm^{-1} corresponded to Mo-O-Ni stretching vibration modes in NiMoO_4 species,^{22, 23} while the whole of above bands shift downward with the increase of Co concentration in samples. Finally, the peaks located at around 938 cm^{-1} , 875 cm^{-1} , 819 cm^{-1} , 703 cm^{-1} and 366 cm^{-1} attributed to Mo-O-Co are observed in the spectrum of CoMoO_4 .²⁴ In addition, the band at 329 cm^{-1} can be assimilated to MoO_4 vibrations.¹⁹ The above results demonstrate that the $\text{NiMoO}_4@\text{CoMoO}_4$ hybrid composites directly grown on nickel foam substrate have been successfully synthesized via a simple hydrothermal process.

The morphologies of products are further investigated by SEM. Figure 2 (a, b) shows the SEM images of the pristine nickel foam. The nickel template with crosslink structure presents numerous pores, and their sizes range from 200 to 500 μm (Inset Figure 2(a)), and only Ni element is found in the EDS spectrum (Figure S1). The low-magnification SEM images in Figure 2(c, d) depict that the $\text{NiMoO}_4@\text{CoMoO}_4$ hierarchical nanospheres with Ni/Co molar ratio of 8:2 are uniformly distributed on the skeleton of the nickel foam after facile hydrothermal procedure. According to the higher magnification SEM images (Figure 2(e, f)), the diameter of resulting nanospheres is around $1.5\mu\text{m}$. Interestingly, it can be clearly seen that such nanospheres are built up of many ultrathin nanosheets. These nanosheets with a thickness of about 50 nm are bended, crumpled and connected to each other, forming a unique stable hierarchical structure, which may provide abundant space and electrocative sites, making them fully accessible to electrolyte. Next, the unique architecture and hierarchical feature of $\text{NiMoO}_4@\text{CoMoO}_4$ nanospheres are further confirmed by TEM. Figure 3(a) demonstrates that the nanospheres are constructed by continuous sheet-like structure with relatively thin thickness, which is consistent with the SEM results. The high-resolution TEM (HRTEM) images shown in Figure 3(b) reveals a distinct set of visible lattice fringe with inter-planar distances of 0.30 nm corresponding to the (220) planes of NiMoO_4 . Moreover, the corresponding selected area electro diffraction (SAED) pattern (Figure S (7)) indicates the polycrystalline nature of the nanosheets and presents well-defined diffraction rings. Besides, the

energy dispersive X-ray spectroscopy (EDS) measurement (inset Figure 3(b)) is also conducted to determine the composition of the as-prepared NiMoO₄@CoMoO₄ nanospheres. Except the C and Cu elements attributed to the copper grid substrate, several peaks associated with Ni, Co, Mo and O elements are observed in this spectrum (Figure 3(d)), suggesting that the sample is composed of mainly Ni, Co, Mo and O, which is in good accordance with XRD results.

The SEM images of pure NiMoO₄ (Figure S2), CoMoO₄ (Figure S5) and NiMoO₄@CoMoO₄ products with different Ni/Co molar ratios of 5:5 (Figure S3) and 2:8 (Figure S4) are also provided. Similarly, the whole samples show hierarchical nanoshepere structure, which are constituted by adjacent nanosheets and uniformly covered on the surface of nickel foam. As for the hybrid of NiMoO₄@CoMoO₄, the thickness of nanosheets exhibits a gradual increase along with the raise of Co molar ratio in raw materials and the nanosheets of pure CoMoO₄ present the maximum thickness (about 150 nm), which is shown in Figure S5(d). Meanwhile, the shape of sole CoMoO₄ structure delivers more irregular spherical with rough surface compared to those of other samples. Besides, the energy dispersive X-ray spectroscopy (EDS) measurements are also conducted to determine the composition of the as-prepared NiMoO₄@CoMoO₄ nanospheres. In order to avoid the impact of Ni element resulted from nickel foam substrate, the NiMoO₄@CoMoO₄ nanospheres are scratched from nickel foam for further identification. Several peaks associated with Ni, Co, Mo and O elements are observed in this spectrums of hybrid NiMoO₄@CoMoO₄ samples (Figure S6(b, c, d)), suggesting that the composites are composed of mainly Ni, Co, Mo and O, which is in good accordance with XRD results. In addition, the Co element is absent in pure NiMoO₄ (Figure S6(a)) and there is not the presence of Ni element in sole CoMoO₄ nanospheres (Figure S6(e)).

The surface chemical composition of the hybrid sample can be further identified by XPS, as shown in Figure 4. Clearly, four peaks are observed in Ni 2p core level spectrum (Figure 4 (a)). The binding energy peaks at 856.1 eV and its satellite peaks at 862.4 eV can be assigned to the Ni 2p_{3/2} level, whereas the binding peaks at 873.8 eV and its satellite peaks at 880 eV correspond to the Ni 2p_{1/2} level. The two main

peaks are separated by 17.7 eV, proving the existence of Ni²⁺ oxidation state.²⁵ The Co 2p core level spectrum shows two main peaks with binding energy peaks located at 781.9 and 797.2 eV, belong to Co 2p_{3/2} and Co 2p_{1/2} respectively (Figure 4 (b)).¹⁹ In addition, two peaks with binding energies of 232.2 eV and 235.3 eV corresponding to Mo 3d_{5/2} and Mo 3d_{3/2} respectively are all observed in Mo 3d core level spectrum (Figure 4 (c)).²⁴ Specially, the spectrum of O 1s shows the unique peak at 531.4 eV, which is typical of metal-oxygen bonds.²⁵ The above results suggest the successful fabrication of NiMoO₄@CoMoO₄ hybrid nanospheres. Besides, the N₂ adsorption-desorption isotherms and the corresponding Barrett-Joyner-Halenda (Bjh) pore size distributions curves of the NiMoO₄@CoMoO₄ hybrid nanospheres with Ni/Co ratio of 4:1 are shown in Figure 5. Nitrogen adsorption-desorption results reveal that the hybrid structure possess a BET surface area of 27.9 m²g⁻¹, and BJH plots indicates the average pore size is about 8 nm with a pore volume of 0.054 cm³g⁻¹. Such unique nanostructures are very beneficial to accelerating ions diffusion and electron transportation, making a significant contribution to a high electrochemical performance.

3.2 Electrochemical performance

Figure 6 (a) shows the typical CV curves of pristine nickel foam, pure NiMoO₄, sole CoMoO₄ and NiMoO₄@CoMoO₄ products with various Ni/Co molar ratios at the scan rate of 10 mVs⁻¹ within the potential ranging from 0 to 0.6 V. Obviously, the current density of pure NF is much lower than other electrodes, suggesting that its capacitance contribution is almost negligible.²⁶ Apparently, the CV curves of the resulting NiMoO₄@CoMoO₄ electrodes supply typical pseudocapacitive characteristics with a pair of well-defined redox peaks originating from Faradaic redox reactions related to Ni²⁺/Ni³⁺ and Co²⁺/Co³⁺ couples mediated by OH⁻ ions in alkaline electrolyte,²⁷ which is distinct from that of EDLCs characterized by nearly rectangular shape.²⁸ According to the CV curves, Table 1 includes the anodic and reductive peaks potentials of NiMoO₄@CoMoO₄ nanospheres prepared with different Ni/Co molar ratios. As for pure NiMoO₄ structure, the anodic potential is at around

0.492 V related to the oxidation process and the cathodic peak is at about 0.171 V due to its reverse procedure, which is higher than that of sole CoMoO_4 (0.375 V and 0.091 V respectively). Interestingly, the data suggests that both anodic and reductive peaks shift to lower potential with the increase of Co concentration.

Figure 6 (b) shows the CV curves of $\text{NiMoO}_4@\text{CoMoO}_4$ nanospheres with Ni/Co molar ratio of 8:2 at various scan rates (2, 5, 10, 20 and 30 mVs^{-1}). Even at a high scan rate of 30 mVs^{-1} , the shape of CV curve with a pair of apparent redox peaks maintains well, indicating its desirable pseudocapacitive properties. Moreover, with the gradual increase of scan rates, the anodic and cathodic peaks shift toward the positive and negative potential respectively, mainly attributed to the resistance and the strengthened electrical polarization of the electrode materials.²⁹ Besides, the linear relationship of the square root of the scan rate dependence of the oxidation peak current at different scan rates is shown in Figure 6 (c), proving that the electrode redox reaction is related to a quasi-reversible and diffusion-controlled process.³⁰ Figure 6 (d) presents the charge-discharge plots of $\text{NiMoO}_4@\text{CoMoO}_4$ nanospheres within a potential range of 0-0.5V at different current densities (2, 3, 4, 6, 8, 10, 12 and 16 Ag^{-1}), which is composed of a first potential drop resulted from the internal resistance of electrode and the subsequent evident plateau region corresponding to pseudocapacitive behavior.

In order to further compare and analyze the influence of Ni/Co molar ratios on electrochemical performance of $\text{NiMoO}_4@\text{CoMoO}_4$ hybrid products, a series of Ni/Co molar ratios dependent experiments are performed and their relative CV curves and charge-discharge plots are also supplied in Figure 7. The well-defined a pair of redox peaks are observed even at a high scan rate of 30 mVs^{-1} for sole NiMoO_4 , which is shown in Figure 7 (a). However, it should be noted that under a high scan rate there is a gradual change for the shape of CV curves along with the increase of Co concentration and the anodic and reductive peaks are not distinct especially for pure CoMoO_4 (Figure 7 (g)). Similarly, according to the charge-discharge plots (Figure 7 (b, d, f, h)), the charge-discharge platform at the same current density becomes steeper with the increase of proportion of Co^{2+} in raw solution, which is

consistent with the CV results. The specific capacitance for electrodes can be evaluated from charge-discharge curves according to the equation: $C = (I \times \Delta t) / (m \times \Delta V)$, where C (Fg^{-1}) is the specific capacitance of the electrode based on the mass loading of active materials, I (A) is the current during discharge process, Δt (s) is the discharge time, ΔV (V) is the potential window.³¹ Figure 8 (a) shows the calculated specific capacitance values of NiMoO_4 , CoMoO_4 and $\text{NiMoO}_4@ \text{CoMoO}_4$ composites with different Ni/Co molar ratios at various current densities. The pure NiMoO_4 electrode delivers a specific capacitance of 1116 Fg^{-1} at 2 A g^{-1} , which is larger than that of CoMoO_4 (979.6 Fg^{-1}), however less than those of $\text{NiMoO}_4@ \text{CoMoO}_4$ hybrid electrodes. More importantly, the composite with Ni/Co mass ratio of 8:2 shows the best specific capacitance (1601.6 Fg^{-1}), as well as the highest capacitance of 867.2 Fg^{-1} even at a high current density of 16 Ag^{-1} (about 54.1% retention), suggesting its excellent rate capability. It is worth mentioning that the results in this work are also higher than those in other previously reported BMTOs (as shown in Table 2).^{18, 19, 32-35} Comparably, the samples with Ni/Co molar ratios of 10:0, 5:5, 2:8 and 0:10 can only retain 41%, 49.7%, 46.6% and 45%, respectively, when the charge-discharge current density changes from 2 to 16 Ag^{-1} . After comprehensive consideration, we can draw a conclusion that the resulting $\text{NiMoO}_4@ \text{CoMoO}_4$ nanocomposites could combine the advantages of high specific capacitance of NiMoO_4 and the good rate capability of CoMoO_4 , which may be a promising candidate for practical applications for supercapacitors.

As a critical parameter to determine the energy storage performance for practical applications, the long-term cycling stability tests are conducted by continuous charge-discharge experiments for 2000 cycles at the current density of 6 Ag^{-1} , which is shown in Figure 8 (b). Although the $\text{NiMoO}_4@ \text{CoMoO}_4$ nanospheres electrode ($n(\text{Ni})/n(\text{Co})=8:2$) exhibits a small fading of capacitance, which is may mainly originated from the exfoliation of the active material during the ion insertion/removal process for long time cycling, the final specific capacitance after 2000 cycles is still able to achieve 812 Fg^{-1} , which is much larger than those of other samples with different Ni/Co molar ratios of 10:0 (324 Fg^{-1}), 5:5 (400.2 Fg^{-1}), 2:8 (456.3 Fg^{-1}) and

0:10 (420.8 Fg^{-1}). The last twenty charge-discharge curves of $\text{NiMoO}_4@\text{CoMoO}_4$ nanospheres with $n(\text{Ni})/n(\text{Co})=8:2$ are displayed (inset Figure 8 (b)), wherein the pseudocapacitive characteristic of charge-discharge plots is still distinct. As can be seen in Figure 8 (c), the little exfoliation of active material is observed, however the nanosphere structure of $\text{NiMoO}_4@\text{CoMoO}_4$ with interconnected sheets are retained well, as shown in Figure 8 (d).

The electrochemical impedance spectrum (EIS) is further carried out to investigate the electrochemical behaviors of the resulting materials and the Nyquist plots are provided in Figure 9 (a). Obviously, a semicircle section at high frequency region corresponding to the charge-discharge resistance (R_{ct}) caused by Faradaic reactions and the double-layer capacitance (C_{dl}) on the surface, and a straight line ascribed to the Warburg impedance (Z_w) related to the diffusion of electrolyte to the electrode surface are all observed.³⁶ Besides, according to the partial enlarged Nyquist plots (inset Figure 9), the $\text{NiMoO}_4@\text{CoMoO}_4$ hybrid product with the Ni/Co molar ratio of 8:2 exhibits the lowest equivalent series resistance (R_s) of 1.63Ω , which is calculated from the intercept of the real axis at high-frequency, including the inherent resistance of the electroactive material, the bulk resistance of electrolyte, the contact resistance at the active material/current collector interface.³⁷

The CV curves of the two-electrode supercapacitor device (as illustrated in Figure 10 (a)) at different scan rates are depicted in Figure 10 (b). Charge-discharge measurements are also applied at different current densities to evaluate the electrochemical properties and calculate the specific capacitance (Figure 10 (c)). According to the discharge plots, the device shows a high specific capacitance of 112.2 Fg^{-1} at the current density of 2 Ag^{-1} , as well as a capacitance of 77.4 Fg^{-1} even at the density of 14 Ag^{-1} , which is better than that of other reported results^{38,39}. In addition, Figure S 8 exhibits the Ragone plot of the two-electrode device. Figure 10 (d) reveals the cycling performance of the symmetric supercapacitor up to 2000 times. Although the specific capacitance decreases fast at the beginning, it keeps steady from 200th to 2000th cycle, and finally about 83% of the initial capacitance is retained after 2000 cycles.

On the basis of above results, the NiMoO₄@CoMoO₄ hierarchical nanospheres with Ni/Co molar ratio of 8:2 anchored randomly on nickel foam would be applied as binder-free electrodes for supercapacitor applications. The excellent electrochemical performance can be mainly attributed to their multiple merits: (1) Both NiMoO₄ and CoMoO₄ are good pseudocapacitive materials in KOH electrolyte, hence contributing to the electrochemical activity. (2) The electrode composed of multi-component materials can make use of synergistic effects from individual constituents, presenting multiple oxidation states. (3) The high electrical conductivity of metal molybdates is advantageous for fast electron transportation. (4) The direct deposition on nickel foam with good adhesion would avoid the use of polymer binder and conducting additives, efficiently reduce Ohmic polarization and improve the rate capability. (5) Furthermore, the unique hierarchical sphere-like structure assembled with thin nanosheets (inset Figure 10 (d)) could provide efficient ion and electron transport, giving rise to the faster redox reaction and result in high specific capacitance even at high current densities.

4. Conclusion

In summary, we have demonstrated the design and fabrication of NiMoO₄@CoMoO₄ hierarchical nanospheres electrode by a facile hydrothermal method. We have investigated the structures, morphologies and electrochemical properties of the nanocomposites prepared with different Ni:Co ratios in raw materials. The composite synthesized with the molar ratio of 8:2 (Ni:Co) combining the advantages of both NiMoO₄ and CoMoO₄ delivers a maximum specific capacitance of 1601.6 Fg⁻¹ at a current density of 2 Ag⁻¹, as well as good rate capability and a superior cycle life, which is attributed to the high electrical conductivity of metal molybdates, multi oxidation states, the unique sphere-like microstructure, binder-free electrode design and the synergistic effects of nickel and cobalt to the overall electrochemical performance. The performance we achieved evidently guarantees the great potential of the NiMoO₄@CoMoO₄ nanocomposite in various energy storage technologies.

Acknowledgments

This work was supported by the Grants from National Natural Science Foundation of China (Nos. 51002129 and 11204262), Open Fund based on innovation platform of Hunan colleges and universities (No. 13K045 and 12K045), Provincial Natural Science Foundation of Hunan (No. 14JJ3079), Hunan Provincial Innovation Foundation For Postgraduate (No. CX2014B263 and No. CX2014A011) and the China Postdoctoral Science Foundation funded project (No. 20100480068).

References

1. J. Zhu, D. Yang, Z. Yin, Q. Yan and H. Zhang, *Small*, 2014, 10, 3480-3498.
2. Y. Li, Z. Li and P. K. Shen, *Advanced Materials*, 2013, 25, 2474-2480.
3. Y. Gogotsi and P. Simon, *Science Magazine*, 2011, 334, 917-918.
4. Q. An, P. Zhang, Q. Wei, L. He, F. Xiong, J. Sheng, Q. Wang and L. Mai, *Journal of Materials Chemistry A*, 2014, 2, 3297-3302.
5. X. Cao, Z. Yin and H. Zhang, *Energy & Environmental Science*, 2014, 7, 1850-1865.
6. X. Cao, Y. Shi, W. Shi, G. Lu, X. Huang, Q. Yan, Q. Zhang and H. Zhang, *Small*, 2011, 7, 3163-3168.
7. J. Pu, Z. Wang, K.-L. Wu, N. Yu and E. Sheng, *Physical Chemistry Chemical Physics*, 2013.
8. Y. Li, L. Cao, L. Qiao, M. Zhou, Y. Yang, P. Xiao and Y. Zhang, *Journal of Materials Chemistry A*, 2014, 2, 6540.
9. Q. Lu, J. G. Chen and J. Q. Xiao, *Angewandte Chemie International Edition*, 2013, 52, 1882-1889.
10. Y.-T. Kim, K. Tadai and T. Mitani, *Journal of Materials Chemistry*, 2005, 15, 4914-4921.
11. Y. Zhang, L. Li, H. Su, W. Huang and X. Dong, *Journal of Materials Chemistry A*, 2015, 3, 43-59.
12. D. Guo, H. Zhang, X. Yu, M. Zhang, P. Zhang, Q. Li and T. Wang, *Journal of Materials Chemistry A*, 2013, 1, 7247.
13. Y. Cao, W. Li, K. Xu, Y. Zhang, T. Ji, R. Zou, J. Yang, Z. Qin and J. Hu, *Journal of Materials Chemistry A*, 2014, 2, 20723-20728.
14. L.-Q. Mai, F. Yang, Y.-L. Zhao, X. Xu, L. Xu and Y.-Z. Luo, *Nature Communications*, 2011, 2, 381.
15. D. Cai, D. Wang, B. Liu, L. Wang, Y. Liu, H. Li, Y. Wang, Q. Li and T. Wang, *ACS applied materials & interfaces*, 2014, 6, 5050-5055.
16. X. Yu, B. Lu and Z. Xu, *Advanced Materials*, 2014, 26, 1044-1051.
17. D. Cai, B. Liu, D. Wang, Y. Liu, L. Wang, H. Li, Y. Wang, C. Wang, Q. Li and T. Wang, *Electrochimica Acta*, 2014, 125, 294-301.
18. B. Senthilkumar, K. Vijaya Sankar, R. Kalai Selvan, M. Danielle and M. Manickam, *RSC Advances*, 2013, 3, 352.
19. K. Xu, J. Chao, W. Li, Q. Liu, Z. Wang, X. Liu, R. Zou and J. Hu, *RSC Advances*, 2014, 4, 34307-34314.
20. S. Peng, L. Li, H. B. Wu, S. Madhavi and X. W. D. Lou, *Advanced Energy Materials*, 2014.
21. Q. Zhang, C. Xu and B. Lu, *Electrochimica Acta*, 2014, 132, 180-185.
22. H. M. Abdel-Dayem, *Industrial & engineering chemistry research*, 2007, 46, 2466-2472.
23. B. Moreno, E. Chinarro, M. Colomer and J. Jurado, *The Journal of Physical Chemistry C*, 2010, 114, 4251-4257.
24. X. Xia, W. Lei, Q. Hao, W. Wang and X. Wang, *Electrochimica Acta*, 2013, 99, 253-261.
25. Z. Yin, S. Zhang, Y. Chen, P. Gao, C. Zhu, P. Yang and L. Qi, *Journal of Materials Chemistry A*, 2015, 3, 739-745.
26. J. Yan, Z. Fan, W. Sun, G. Ning, T. Wei, Q. Zhang, R. Zhang, L. Zhi and F. Wei, *Advanced Functional Materials*, 2012, 22, 2632-2641.
27. B. Senthilkumar, D. Meyrick, Y.-S. Lee and R. K. Selvan, *RSC Advances*, 2013, 3, 16542.

28. X. Liu, X. Qi, Z. Zhang, L. Ren, G. Hao, Y. Liu, Y. Wang, K. Huang, X. Wei, J. Li, Z. Huang and J. Zhong, *RSC Advances*, 2014, 4, 13673-13679.
29. Z. Zhang, X. Liu, X. Qi, Z. Huang, L. Ren and J. Zhong, *RSC Advances*, 2014, 4, 37278-37283.
30. Z. Zhang, Z. Huang, L. Ren, Y. Shen, X. Qi and J. Zhong, *Electrochimica Acta*, 2014.
31. J. Xu, L. Gao, J. Cao, W. Wang and Z. Chen, *Electrochimica Acta*, 2010, 56, 732-736.
32. X.-J. Ma, L.-B. Kong, W.-B. Zhang, M.-C. Liu, Y.-C. Luo and L. Kang, *RSC Advances*, 2014, 4, 17884-17890.
33. N. Padmanathan, K. M. Razeeb and S. Selladurai, *Ionics*, 2014, 20, 1323-1334.
34. D. Cai, D. Wang, B. Liu, Y. Wang, Y. Liu, L. Wang, H. Li, H. Huang, Q. Li and T. Wang, *ACS applied materials & interfaces*, 2013, 5, 12905-12910.
35. Y. Liu, H. Pang, J. Guo, W. Wang, Z. Yan, L. Ma, Y. Ma, G. Li, J. Chen and J. Zhang, *Int. J. Electrochem. Sci*, 2013, 8, 2945-2957.
36. X. Liu, X. Qi, Z. Zhang, L. Ren, Y. Liu, L. Meng, K. Huang and J. Zhong, *Ceramics International*, 2014, 40, 8189-8193.
37. H. Huo, Y. Zhao and C. Xu, *Journal of Materials Chemistry A*, 2014, 2, 15111-15117.
38. A. D. Jagadale, V. S. Kumbhar, D. S. Dhawale and C. D. Lokhande, *Electrochimica Acta*, 2013, 98, 32-38.
39. K. Karthikeyan, D. Kalpana and N. G. Renganathan, *Ionics*, 2009, 15, 107-110.

Figure Captions:

Figure 1. XRD patterns (a) and Raman spectra (b) of NiMoO₄@CoMoO₄ hybrid.

Figure 2. SEM images of pure nickel foam (a,b) and NiMoO₄@CoMoO₄ nanospheres with Ni/Co molar ratio of 8:2 (c-f).

Figure 3. Typical TEM images of NiMoO₄@CoMoO₄ nanospheres (Inset (b) are the HRTEM (up) and EDS (down)).

Figure 4. XPS spectra of (a) Ni 2p, (b) Co 2p, (c) Mo 3d and (d) O 1s for NiMoO₄@CoMoO₄ hybrid.

Figure 5. N₂ adsorption-desorption isotherm and pore size distribution (Inset) of the NiMoO₄@CoMoO₄.

Figure 6. (a) CV curves of pure nickel foam and NiMoO₄@CoMoO₄ hybrid with different Ni/Co molar ratios at 10 mVs⁻¹; (b) CV curves at various scan rates of 2, 5, 10, 20 and 30 mVs⁻¹, (c) plots of current vs. the square root of scan rates and (d) charge-discharge curves at different current densities for NiMoO₄@CoMoO₄ nanosphere obtained with Ni/Co molar ratios of 8:2.

Figure 7. CV curves and galvanostatic discharge plots of NiMoO₄@CoMoO₄ nanosphere with different Ni/Co molar ratios of raw materials: 10:0 (a, b), 5:5 (c, d), 2:8 (e, f) and 0:10 (g, h).

Figure 8. Specific capacitances (a) and cycling stability measured at 6 Ag⁻¹ (b) of NiMoO₄@CoMoO₄ nanosphere (Inset is the galvanostatic charge-discharge curves of the last twenty cycles for Ni/Co molar ratio of 8:2); (c-d) SEM images for sample with Ni/Co molar ratio of 8:2 after 2000 cycles.

Figure 9. Nyquist plots of NiMoO₄@CoMoO₄ nanosphere (The inset are the partial enlarged Nyquist plots).

Figure 10. (a) Schematic illustration of symmetric supercapacitor configuration; (b) Cyclic voltammetry curves at various scan rates; (c) discharge curves of the symmetric supercapacitor at various current densities and (d) cycling stability of the symmetric suercapacitor (Inset is the schematic illustration of the basis for the excellent electrochemical performance of NiMoO₄@CoMoO₄ nanospheres).

Table 1. Cathodic and reductive peak potentials of NiMoO₄@CoMoO₄ nanosphere prepared with different Ni/Co molar ratios at 10 mVs⁻¹.

Table 2. Electrochemical performances of BTMOs in previous reports.

Figure 1.

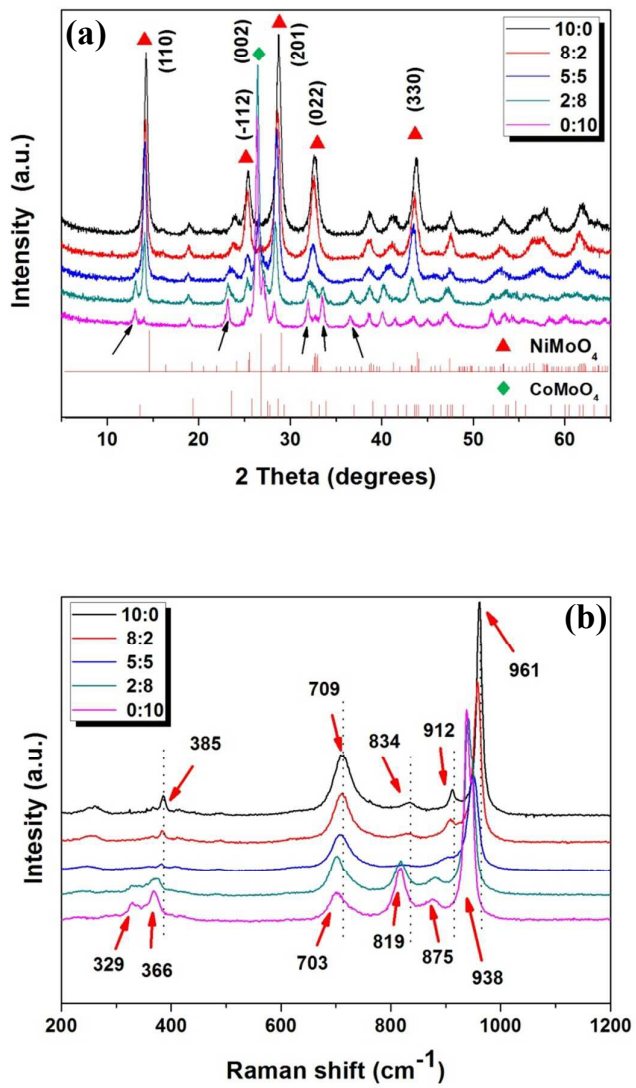


Figure 2.

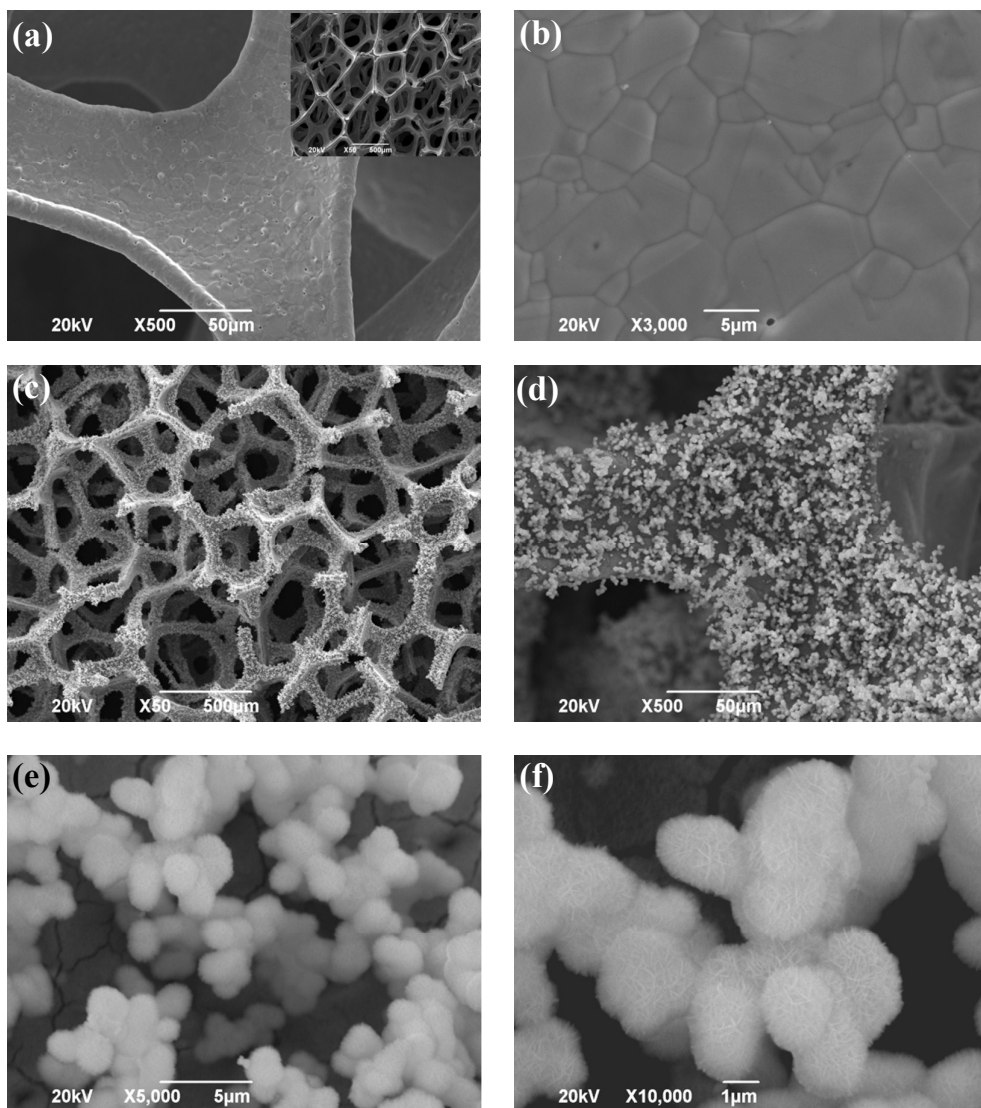


Figure 3

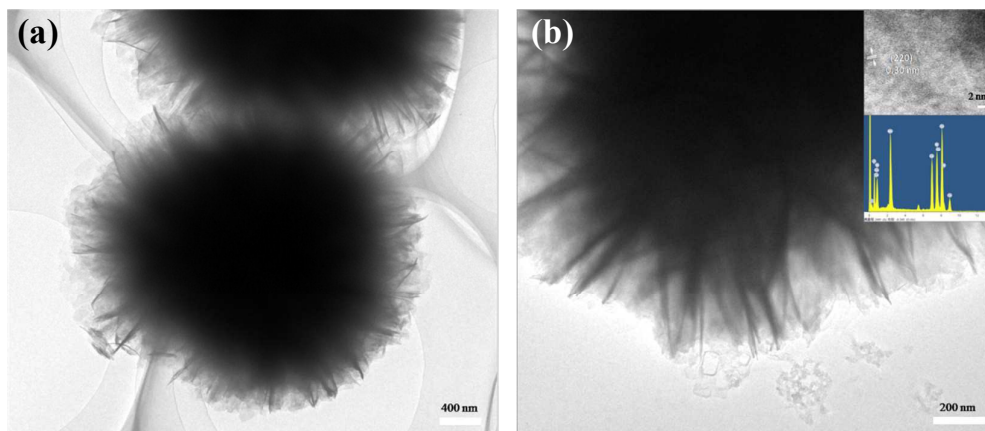


Figure 4

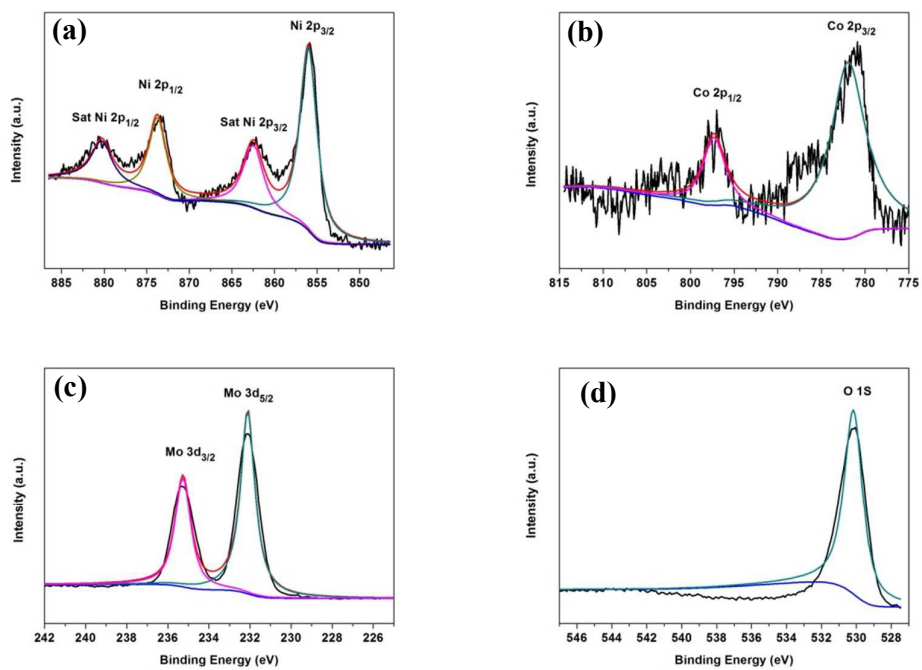


Figure 5

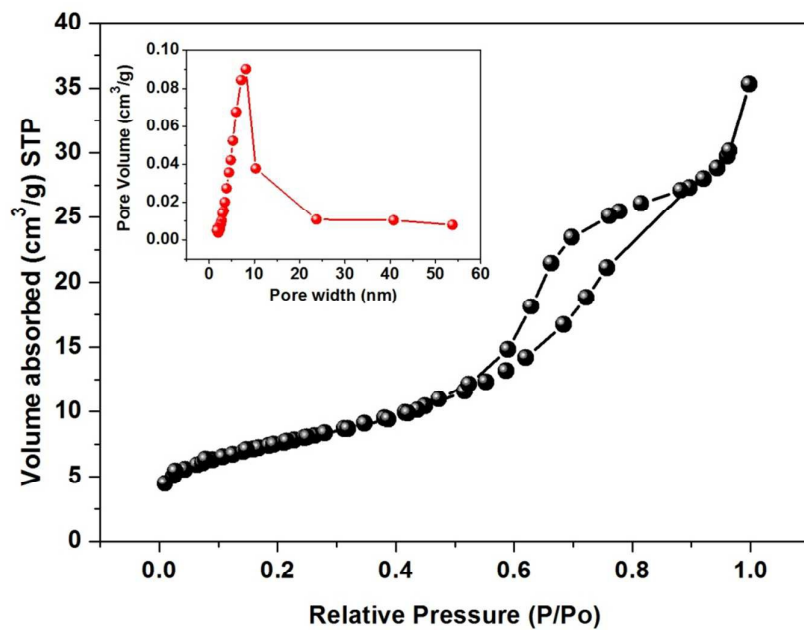


Figure 6

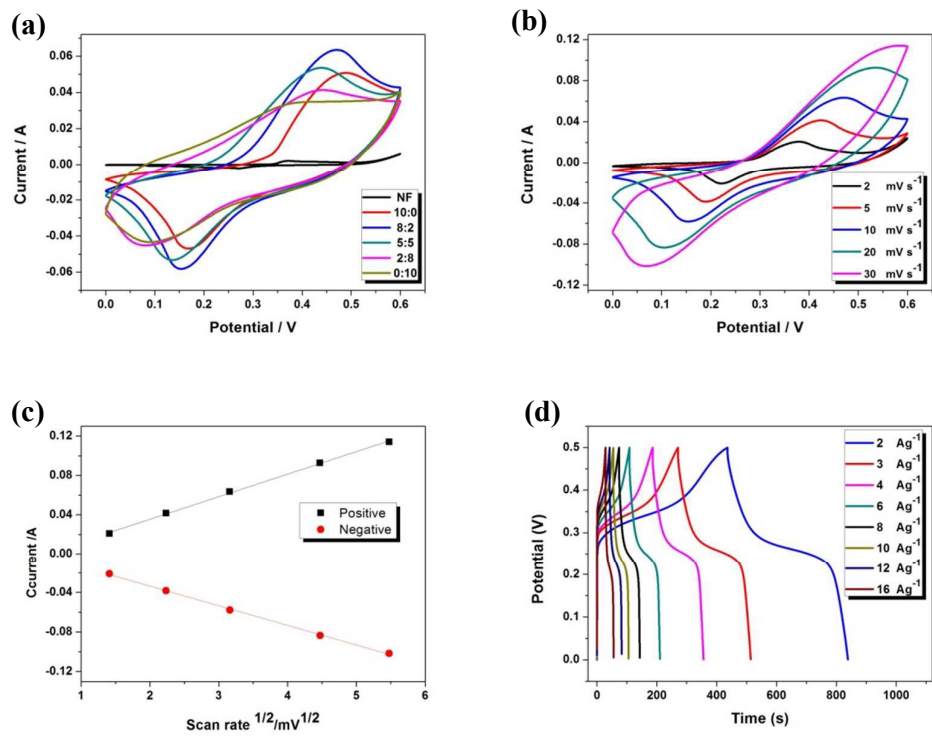


Figure 7

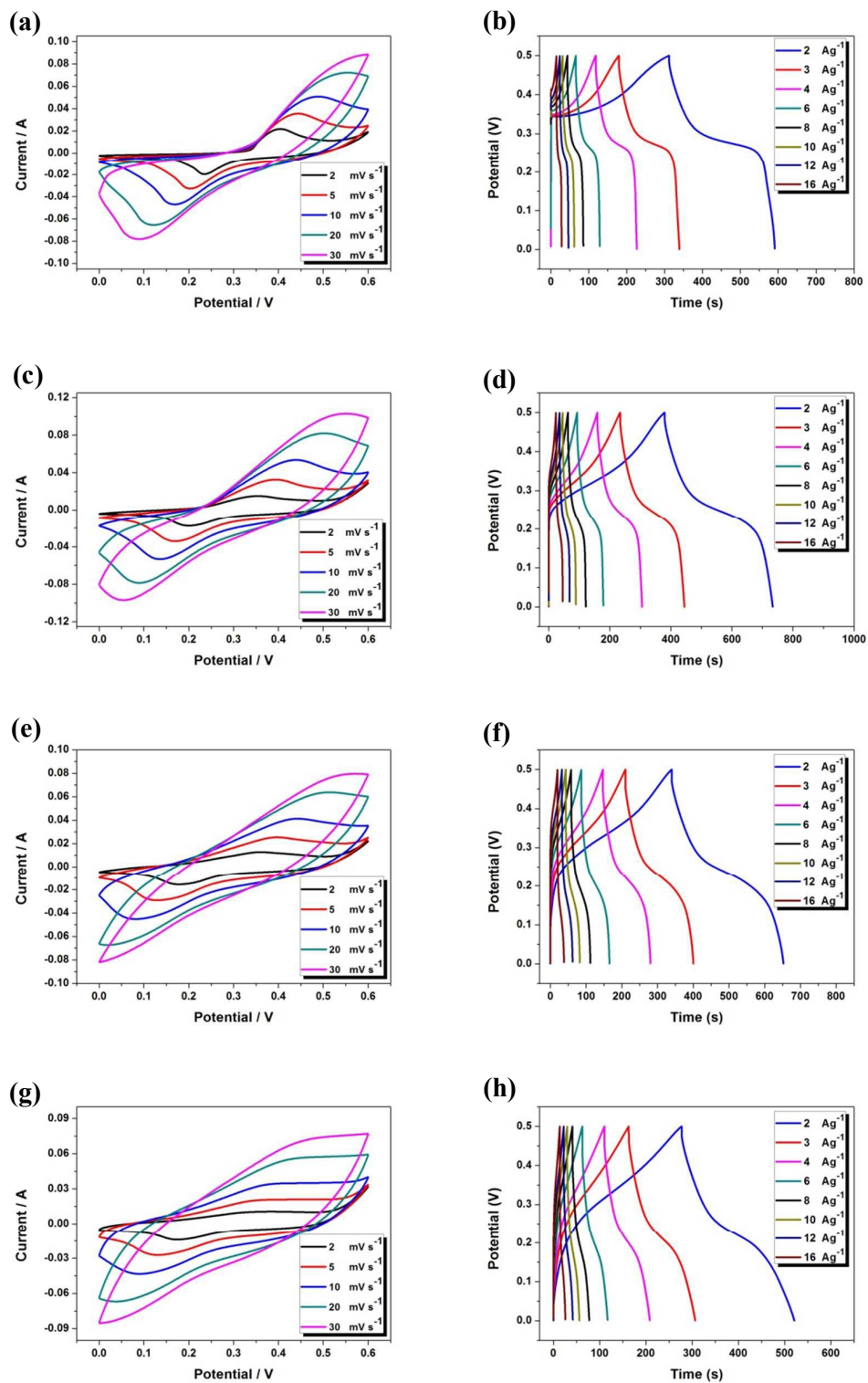


Figure 8

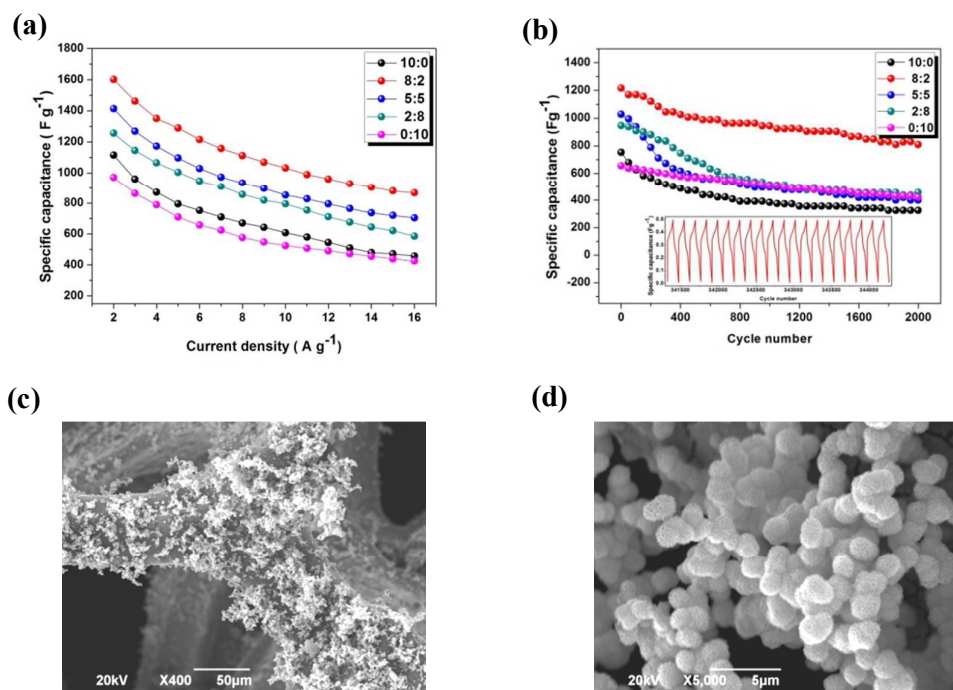


Figure 9

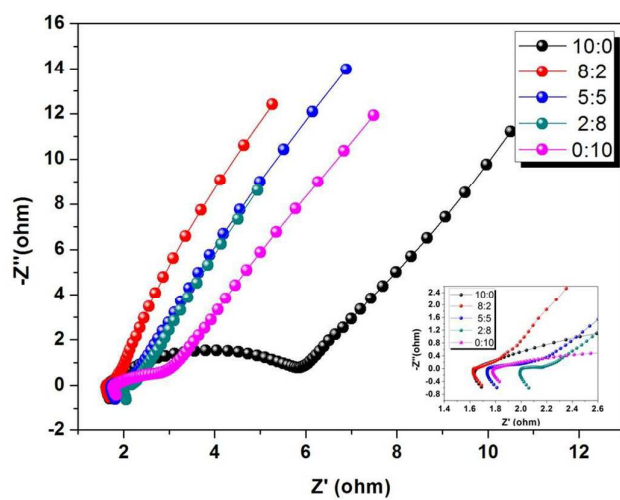


Figure 10

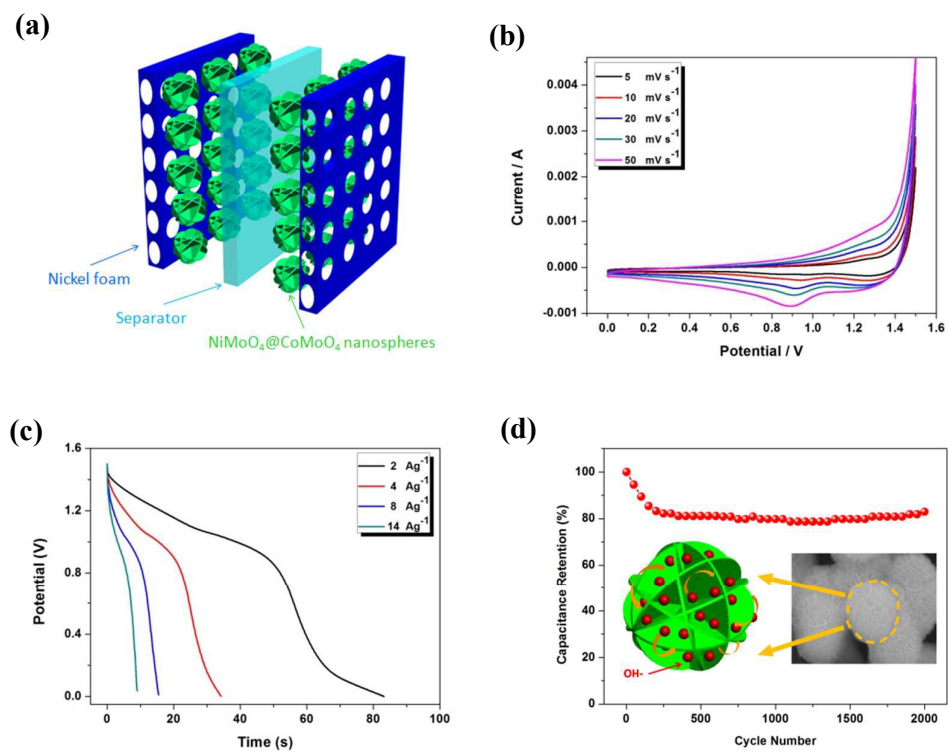


Table 1:

Ni/Co molar ratios	10:0	8:2	5:5	2:8	0:10
Anodic peaks	0.492	0.471	0.449	0.441	0.375
Reductive peaks	0.171	0.153	0.135	0.081	0.091

Table 2.

Materials	Specific capacitance	Ref.
NiMoO ₄ @CoMoO ₄	1601.6 Fg ⁻¹ (2 Ag ⁻¹)	This work
NiO@CoMoO ₄	835 Fg ⁻¹ (2 Ag ⁻¹)	32
CoMoO ₄ /C	451.6 Fg ⁻¹ (1 Ag ⁻¹)	33
CoMoO ₄ ·H ₂ O/rGO	802.2 Fg ⁻¹ (1 Ag ⁻¹)	18
NiMoO ₄ nanospheres	701.9 Fg ⁻¹ (2 Ag ⁻¹)	34
α-NiMoO ₄	1517 Fg ⁻¹ (1.2 Ag ⁻¹)	17
Co _{0.5} Ni _{0.5} MoO ₄ ·nH ₂ O	1040.7 Fg ⁻¹ (0.625 Ag ⁻¹)	35